

Article

# Evaluation of the Antibacterial Activity of a Geopolymer Mortar Based on Metakaolin Supplemented with TiO<sub>2</sub> and CuO Particles Using Glass Waste as Fine Aggregate

Ruby Mejía-de Gutiérrez <sup>1,\*</sup> , Mónica Villaquirán-Caicedo <sup>1</sup> , Sandra Ramírez-Benavides <sup>1</sup>, Myriam Astudillo <sup>2</sup> and Daniel Mejía <sup>2</sup>

<sup>1</sup> Composites Materials Research Group (CENM), Universidad de Valle, calle 13 #100-00 Cali, Colombia; monica.villaquiran@correounivalle.edu.co (M.V.-C.); sandra.ramirez@correounivalle.edu.co (S.R.-B.)

<sup>2</sup> Biotechnology and Bacterial Infections Research Group, Universidad de Valle, calle 4b #36b-37, Cali, Colombia; myriam.astudillo@correounivalle.edu.co (M.A.); daniel.mejia@correounivalle.edu.co (D.M.)

\* Correspondence: ruby.mejia@correounivalle.edu.co

Received: 29 December 2019; Accepted: 6 February 2020; Published: 9 February 2020



**Abstract:** Metakaolin-based geopolymer cements were produced by alkaline activation with a potassium hydroxide and potassium silicate solution. To produce the geopolymer composites, 10 wt.% titanium oxide (TiO<sub>2</sub>) and 5 wt.% copper oxide (CuO) nanoparticles were used. The geopolymer mortar was prepared using glass waste as fine aggregate. The raw materials and materials produced were characterized by X-ray diffraction, electron microscopy, and Fourier-transform infrared spectroscopy techniques. Likewise, the geopolymer samples were characterized to determine their physical properties, including their density, porosity, and absorption. The photocatalytic activity of the materials was evaluated by activating the nanoparticles in a chamber with UV–Vis light during 24 h; then, different tests were performed to determine the growth inhibition of *Staphylococcus aureus*, *Escherichia coli*, and *Pseudomonas aeruginosa* bacteria in nutrient agar for times of up to 24 h. The study results showed that a geopolymer mortar containing glass waste as fine aggregate (GP-G) exhibited a water absorption 56.73% lower than that of the reference geopolymer paste without glass (GP). Likewise, glass particles allowed the material to have a smoother and more homogeneous surface. The pore volume and density of the GP-G were 37.97% lower and 40.36% higher, respectively, than those of the GP. The study with bacteria showed that, after 24 h in the culture media, the GP-G mortars exhibited a high inhibition capacity for the growth of *P. aeruginosa* from solutions of 10<sup>-4</sup> mL and in solutions of 10<sup>-6</sup> mL for *E. coli* and *S. aureus*. These results indicate the possibility of generating antibacterial surfaces by applying geopolymer composite.

**Keywords:** geopolymer; glass waste; titanium oxide; copper oxide; antibacterial surfaces

## 1. Introduction

The problematic relationships between environmental pollution and health preservation and prolongation are a subject of current interest and are, therefore, widely studied. Most health problems are associated with the presence of microorganisms such as bacteria, fungi, protozoa, and viruses that commonly infect humans in the living environment, leading to chronic infections and even leading to mortality [1–3]. The inanimate surfaces of different materials are often described as the source of hospital outbreaks because their contact with different microorganisms allows microbial permanence for a period of time favoring bacterial proliferation, and they are, therefore, reservoirs of bacteria that cause diseases transmitted through surfaces or fomites. This continues to be a cause of great concern

for the medical domain, with a significant economic burden. One of the main causes of morbidity is infection with methicillin-resistant *Staphylococcus aureus* (MRSA) [4,5]. These microorganisms also contribute to severely deteriorating surfaces, greatly reducing the durability and increasing the repair costs of the material [6]. Considering this dynamic, a material with antibacterial surfaces would be ideal to prevent microbial proliferation and, likewise, contamination.

Therefore, surface materials and antibacterial systems are of the utmost importance not only in hospitals and sanitary environments but also for domestic, industrial, and marine applications, among others [7]. Various studies were carried out with the goal of improving the antibacterial capacity of construction materials as glazes on ceramic tiles and pastes based on alkali-activated slag [2,8,9]. Among these construction materials, the use of geopolymers is a great option due to their high alkalinity and ease of functionalization by incorporating semiconductor materials (ZnO, TiO<sub>2</sub>, CuO, and Fe<sub>2</sub>O<sub>3</sub>), which, when exposed to UV and UV-Vis radiation, exhibit a functional activity, i.e., photocatalytic properties [10,11]. One of the most studied semiconductors is titanium dioxide (TiO<sub>2</sub>), a harmless material that is highly resistant to photocorrosion, stable in aqueous solutions, inexpensive, and abundant in nature, which also exhibits a desired high photocatalytic activity under ultraviolet irradiation [9,12–14]. Semiconductor particles as TiO<sub>2</sub>, Fe<sub>3</sub>O<sub>4</sub>, ZnO, and CuO can cause inactivation of bacteria (i.e., elimination of bacteria) and viruses in different types of environments [2,15–17]. These metal oxides were incorporated into the surface of different materials using advanced deposition techniques, such as chemical vapor deposition, ion implantation, sputtering, and electrochemical deposition of a solution. However, these technologies are expensive and difficult to apply to large-volume particles or complex shapes [18].

In general, the antimicrobial activity of CuO and TiO<sub>2</sub> metallic nanoparticles was studied with Gram-positive and Gram-negative bacteria [19–21]. Although the nanoparticles tended to inhibit the bacteria in all cases, it was observed that the effectiveness depends on the morphology and particle size. Hasmaliza et al. [9] evaluated the antibacterial properties of ceramic tiles coated with enamel mixed with anatase TiO<sub>2</sub> by exposing the tiles for different times (0, 2, 4, and 8 h) to the bacterium *Escherichia coli*; the TiO<sub>2</sub> content (5, 10, and 15 wt.%) and particle size of the oxide were also varied, and, at a longer exposure time, the number of colony-forming units (CFUs) decreased. At the same time, the nanometric particle sizes favored the antibacterial properties due to the greater surface area available to contact the bacteria; in contrast, in the presence of a greater amount of TiO<sub>2</sub>, the antibacterial yield was lower [9]. Kumar et al. [20] evaluated the antibacterial activity of a polymer nanocomposite containing TiO<sub>2</sub> and CuO nanoparticles with satisfactory results. Haider et al. [19] evaluated the photocatalytic and antibacterial activity of TiO<sub>2</sub> nanoparticles synthesized via the sol-gel method and calcined at different temperatures (400, 600, 800, and 1000 °C). TiO<sub>2</sub> was exposed to two types of bacteria, *Pseudomonas aeruginosa* and *S. aureus*, and it was 100% effective in eliminating these bacteria under solar irradiation.

Geopolymers based on metakaolin, halloysite clay, and fly ash with TiO<sub>2</sub> nanoparticles reported photocatalytic properties. These materials allow functional ceramics to be produced for self-cleaning ability, removing dyes as B-rhodamine and methylene blue, and leading to nitric oxide degradation [11,22–28]. Nanoparticles are also used in dental applications [10,29]. However, the information on the antibacterial effect of nanoparticles incorporated in geopolymeric pastes or mortars is limited [30]. TiO<sub>2</sub> microparticles (20 and 50 wt.%) and ZnO nanoparticles were incorporated in geopolymer pastes based on metakaolin (MK) [31,32], where the authors reported a bacteriostatic effect in the presence of contaminated water. Similar results were obtained using MK-based geopolymer mortar doped with copper [6]. Geopolymers based on fly ash and calcined baluko shells incorporating Ag nanoparticles were also used to evaluate their antibacterial capacity [33,34]. These studies showed that the nanoparticles can be used to prepare geopolymers with satisfactory inhibition capacity for the growth of bacteria. Additionally, it was reported that Portland cement mortars with added glass containing 2 wt.% TiO<sub>2</sub> and the incorporation of nanosilica exhibited the ability to inhibit *E. coli* growth in just 30 min [35].

The objective of this preliminary study was to determine the effects of incorporating nanoparticles of metallic oxides, such as  $\text{TiO}_2$  and  $\text{CuO}$ , on the antimicrobial potential of a geopolymeric binder based on metakaolin (MK), and its corresponding geopolymer mortar using glass waste as a fine aggregate. Geopolymer mortars were fabricated for their use as coatings of construction elements for environments susceptible to bacterial growth. Among the microorganisms potentially pathogenic to humans were selected Gram-negative bacteria such as *E. coli* and *Pseudomonas aeruginosa* and Gram-positive bacteria such as *S. aureus*. Infections with these bacteria are recurrent and transmissible to people close to each other [4,5,36,37]. In addition, this preliminary study proposes the direct incorporation of such nanoparticles by mechanically mixing the components of the material in order to directly apply the geopolymer mortar on the substrate surfaces instead of using conventional deposition processes to produce oxide coatings.

## 2. Materials and Methods

### 2.1. Materials

To obtain the geopolymer cement paste, the precursor used was metakaolin (MK MetaMax, BASF, Florham Park, NJ, USA). A mixture of a commercial potassium silicate ( $\text{SiO}_2 = 26.38\%$ ,  $\text{K}_2\text{O} = 13.06\%$ ,  $\text{H}_2\text{O} = 60.56\%$ ), analytical grade potassium hydroxide (KOH), and water was used as an alkaline activator. The cementitious material was formulated using the following molar ratios of oxides, as determined by previous studies:  $\text{SiO}_2/\text{Al}_2\text{O}_3 = 2.5$  and  $\text{K}_2\text{O}/\text{SiO}_2 = 0.28$  [38,39]. To produce the geopolymer composite with photocatalytic and antibacterial properties, titanium oxide ( $\text{TiO}_2$ ) and copper oxide ( $\text{CuO}$ ) particles were added. The  $\text{TiO}_2$  used was high-purity and analytical grade (Merck, reference 1008081000). The  $\text{CuO}$  nanoparticles were synthesized from copper acetate ( $(\text{CH}_3\text{COO})_2\text{Cu}\cdot\text{H}_2\text{O}$ ) using the modified Pechini method [40] (Figure 1). To evaluate the cementitious properties, the pastes and mortars were prepared. The mortar was prepared using glass waste (G) as a fine aggregate.

To synthesize the  $\text{CuO}$  nanoparticles, citric acid and ethylene glycol were initially mixed in 100 mL of distilled water, and the mixture was heated to 70 °C. Then, copper acetate was added. These precursors were mixed with a molar ratio of 1:1:2, and the solution was constantly stirred using a magnetic stirrer. Simultaneously, an  $\text{NH}_4\text{OH}$  solution was added until a neutral pH (pH = 7) was obtained. The resulting polymeric resin was subjected to an initial thermal treatment at 350 °C; the thermally treated powder was pulverized using a ceramic mortar. The resulting fine powder was thermally treated at 450 °C. The heating rate used in the two heat treatments was adjusted to 10 °C/min.

### 2.2. Preparation of the Geopolymers

To prepare the geopolymers, the components were firstly mixed in a solid state; then, the activating solution was added. The components were mixed for 15 min using a Hobart mixer. Next, the mixture was poured into silicone molds, and discs with 2.5 cm diameters were prepared. The liquid/solid ratio was 0.35 for the pastes and 0.40 for the mortar. The samples were wrapped with a plastic film to prevent moisture from evaporating and kept for 24 h in a chamber with a relative humidity (RH) >90% and a temperature of 25 °C. Subsequently, the samples were demolded and stored for 28 days. Figure 2 shows the experimental methodology followed in the study in order to prepare the geopolymer composites. Table 1 shows the compositions and codes of the mixtures evaluated. Two geopolymer pastes (GP, mGP) were prepared using 10 wt.% titanium oxide ( $\text{TiO}_2$ ) and 5 wt.% copper oxide ( $\text{CuO}$ ) particles. The percentage of  $\text{TiO}_2$  incorporated was selected based on previous studies [11], where a high photocatalytic capacity for degrading B-rhodamine was achieved using 10 wt.%  $\text{TiO}_2$ . Geopolymer mortars (GP-G) were manufactured with a binder/fine aggregate ratio of 1:2 by weight using glass waste (G) as fine aggregate. The photocatalytic capacity of MK-based geopolymer mortars (GP-G) increased up to 72% compared to that obtained with mortars using natural

sand [41]. Geopolymer mortars with CuO particles were not prepared because the results obtained with the proportion of the oxide used in mGP were negative, as discussed later.

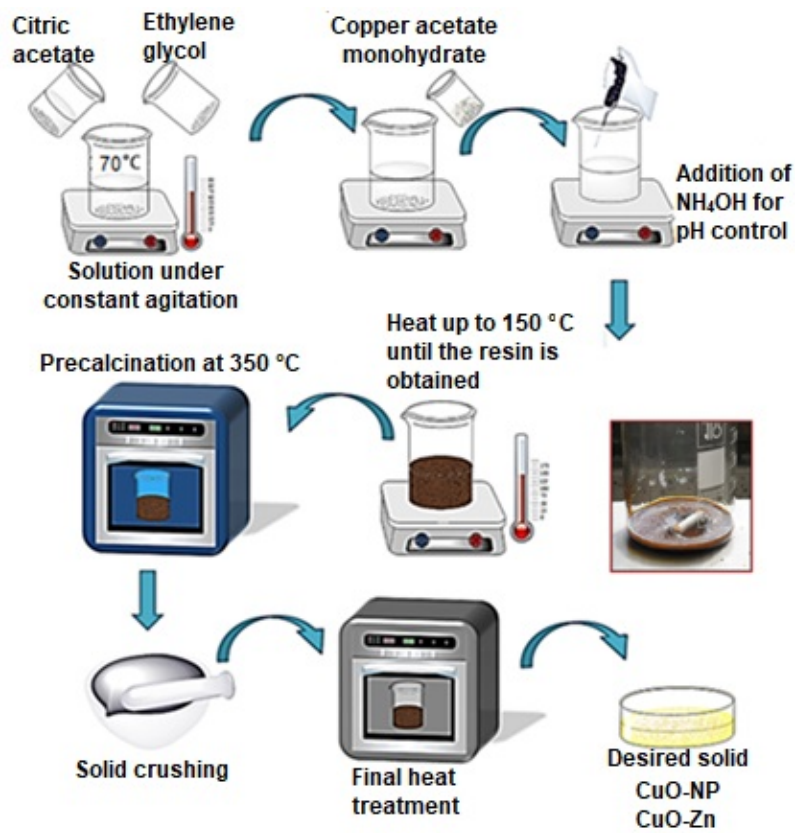


Figure 1. Diagram of the methodology used to synthesize the CuO nanoparticles via the Pechini method.



Figure 2. Diagram of the methodology used to prepare the geopolymer composites.

Table 1. Compositions of the fabricated materials. ID—identifier.

ID	Geopolymer (GP) Type	GP (wt.%)	TiO <sub>2</sub> (wt.%)	CuO (wt.%)
GP	Paste	90	10	0
mGP	Paste	95	0	5
GP-G	Mortar with glass waste (G) as fine aggregate	90	10	0

### 2.3. Physicochemical and Microstructural Characterization Techniques

The following instrumental techniques were used to characterize the materials:

- The chemical composition of the starting materials was determined by X-ray fluorescence (XRF) using a Magix Pro PW-2440 X-ray fluorescence spectrometer (PANalytical, Tollerton, Nottingham, UK) equipped with a rhodium tube with a maximum output of 4.0 kW and 0.02% sensitivity.
- The X-ray diffraction (XRD) patterns were obtained with a RINT2000 wide-angle goniometer using Cu K $\alpha$  radiation at 45 kV and 40 mA, and data were collected with a step size of 0.02° over the range of 5°–60° 2 $\theta$  using a scan speed of 5°/min.
- Fourier-transform infrared spectroscopy (FTIR) was performed with a PerkinElmer Spectrum 100 spectrometer operated in transmittance mode, and data were collected for a wavelength range of 450 cm<sup>-1</sup> to 4000 cm<sup>-1</sup>. The samples were prepared using the compressed KBr method.
- The morphological observations and particle sizes of TiO<sub>2</sub> and CuO were evaluated by scanning electron microscopy (SEM) using a JEOL JSM-6490 LV SEM system operated with an accelerating voltage of 20 kV. The specimens were coated with gold, and the observations were made in vacuum mode.
- The density, pore volume, and water absorption of the geopolymers were determined following the procedures detailed in the ASTM C642-13 standard, except that the temperature used to dry the sample in the oven was 60 °C for 48 h.

### 2.4. Evaluation of the Antibacterial Activity of the Geopolymeric Materials

The geopolymer samples were exposed to the bacteria under study by activating the materials with UV-A light for 48 h. The UV-A radiation was provided by two mercury lamps (Electrolux T8 20 W BLB) located inside a black acrylic dome. The lamps emitted light at an intensity of 10.3 W·m<sup>-2</sup>, which was measured with a Delta Ohm HD 2102.2 Photoradiometer using the filter for UV-A light range ( $k = 360$  nm) at 5 mm [14]. The growth inhibition capacity of the bacteria in the materials was studied using *E. coli*, *S. aureus*, and *P. aeruginosa* bacteria. The tests were performed in two stages. The first stage followed the standard to evaluate the bactericidal capacity with the bacteria to be tested in the GP (with 10 wt.% TiO<sub>2</sub>) and mGP (with 5 wt.% CuO) samples. This initial stage was performed by following the bacterial growth inhibition zone method (disc diffusion agar test). This method consisted of placing the sample, i.e., the GP and mGP disc, in a Petri dish and spreading nutrient agar on the sample. The Petri dishes were then covered for 24 h at 25 °C, and the bacterial growth was verified by the formation of an “inhibition halo” around the disc and under the disc. If the material is favorable to bacterial proliferation, more bacteria would be found at the site where the material rests (Figure 3).

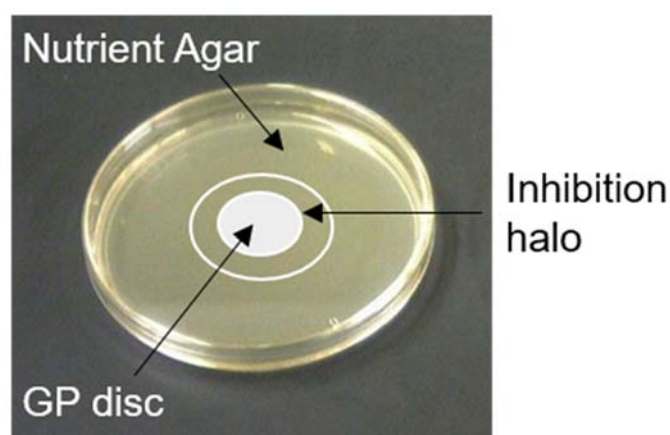


**Figure 3.** Assembly of the nutrient agar method.

By considering the results of the initial stage, the ability of the geopolymer paste (GP) and the mortar with glass (GP-G) to inhibit bacterial growth was evaluated in the second stage. During this stage, the methodology used was based on the Hasmaliza study [9], with a few modifications. The bacteria were cultured in tryptic soya broth (Merck, Darmstadt, Germany) for 24 h. At the beginning of the test, a count was performed in each of the broths by performing six serial dilutions in plate count agar (PCA, Scharlau 01-161). Subsequently, 100  $\mu\text{L}$  of each of the selected bacteria were placed on discs, which were exposed for 2 to 24 h at room temperature (25  $^{\circ}\text{C}$ ) under conditions isolated from contamination. After each of the exposure times, the discs were washed with 5 mL of a 1% peptone-buffered saline solution (Difco, Waltham, MA, USA), which was performed with vigorous stirring for 5 min; finally, the six dilutions were performed in a type-2 laminar flow cabinet (C4, Colombia) to count the number of colony-forming bacteria using the pour plate procedure with PCA. Finally, each agar with its respective inoculum was left in the incubator (WTC Binder, Germany) for 24 h at 37  $^{\circ}\text{C}$  to subsequently count the bacteria grown for each material in the different dilutions.

### 3. Results and Analysis

#### 3.1. Physicochemical and Microstructural Characterization of the Starting Materials and the Produced Geopolymers

The chemical composition of MK and G is shown in Table 2. MK was basically composed of silica and alumina oxides (approximately 97 wt.%) and contains  $\text{TiO}_2$  impurities (1.73 wt.%). This oxide was in the form of anatase, as seen in the XRD results (Figure 4). The results shown in Table 2 indicate that the glass waste used in G was from the  $\text{SiO}_2\text{-Na}_2\text{O-CaO}$  system (calcium sodium glass) and was highly amorphous, as corroborated by the XRD results based on the elevation of the baseline for 2 $\theta$  angles between 20 $^{\circ}$  and 30 $^{\circ}$  (Figure 4).

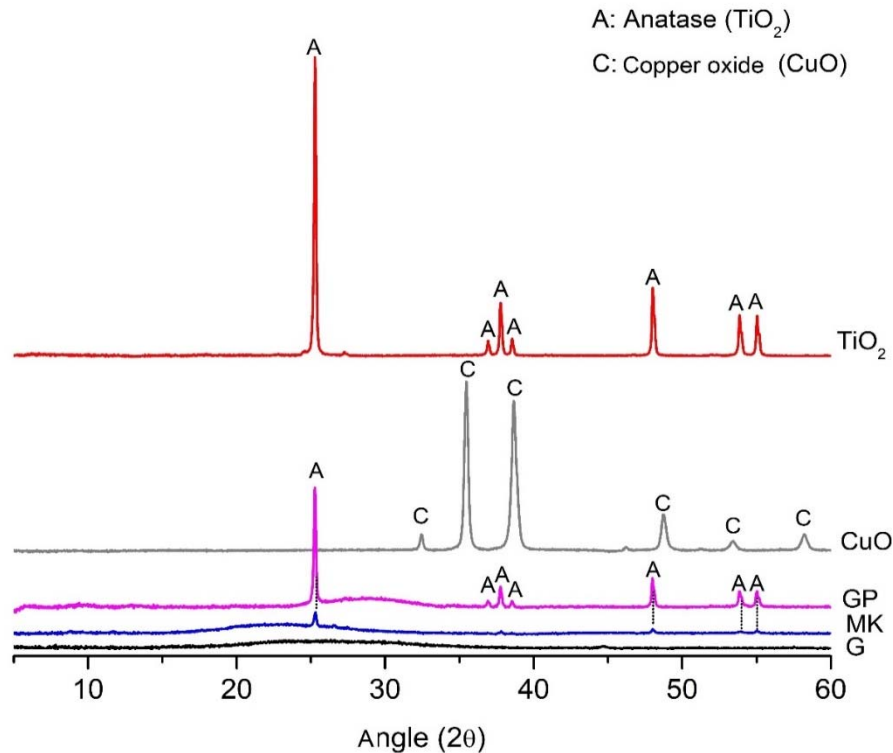


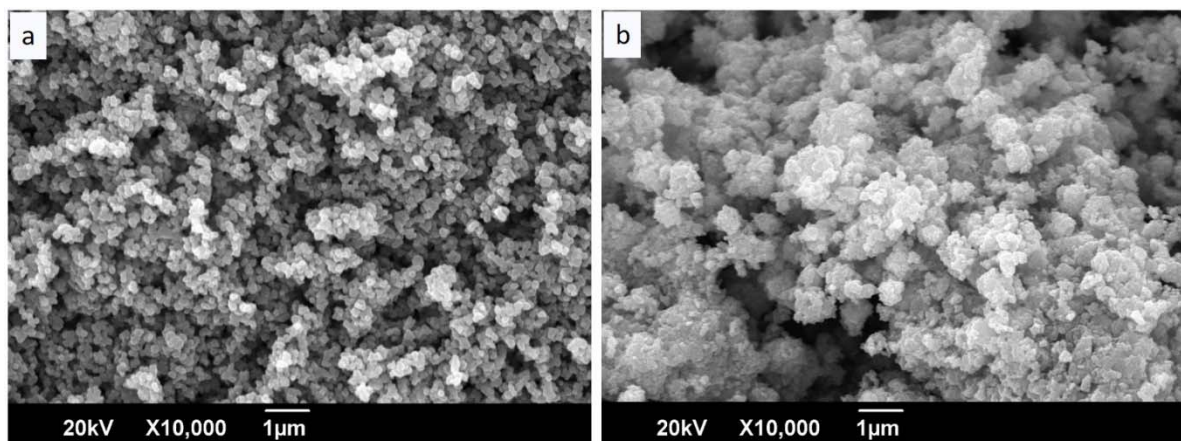
Figure 4. X-ray diffraction (XRD) patterns of the raw materials and GP.

**Table 2.** Chemical composition of metakaolin (MK) and glass waste (wt.%).

Oxide/Material	SiO <sub>2</sub>	Al <sub>2</sub> O <sub>3</sub>	TiO <sub>2</sub>	Fe <sub>2</sub> O <sub>3</sub>	Na <sub>2</sub> O	MgO	K <sub>2</sub> O	P <sub>2</sub> O <sub>5</sub>	CaO	CeO <sub>2</sub>	V <sub>2</sub> O <sub>5</sub>	SO <sub>3</sub>
MK	52.02	44.95	1.73	0.47	0.30	0.19	0.16	0.02	0.02	0.04	0.05	0.05
G	72.27	1.49	–	0.62	13.37	–	–	–	11.15	–	–	–

Titanium oxide existed in the anatase phase (TiO<sub>2</sub>, Inorganic Crystal Structure Database ICSD # 154604), as identified by the peaks observed in the diffractogram (Figure 4) at approximately  $2\theta = 25.3^\circ$ ,  $37.8^\circ$ ,  $48.1^\circ$ ,  $53.9^\circ$ , and  $55.1^\circ$ , which also indicated the high photocatalytic potential of TiO<sub>2</sub>. The XRD pattern of the copper oxide nanoparticles synthesized from copper acetate by the Pechini method showed peaks at  $2\theta = 34^\circ$ ,  $36^\circ$ ,  $38^\circ$ ,  $49^\circ$ ,  $53^\circ$ , and  $58^\circ$ , which corresponded to pure monoclinic CuO (ICSD code 67850), a phase considered to have bactericidal properties [42]. Similar results were found by Román et al. [15]. The XRD pattern obtained for the GP indicated that the material was amorphous (see the lifted baseline for  $2\theta$  between  $25^\circ$  and  $35^\circ$ ), with the only crystalline phase being the anatase phase, which was contributed to a high degree by the TiO<sub>2</sub> particles and to a lesser extent by MK.

SEM was used to determine the particle size of the TiO<sub>2</sub> and CuO particles (Figure 5); the average TiO<sub>2</sub> and CuO particle sizes were 0.615  $\mu\text{m}$  and 0.198  $\mu\text{m}$ , respectively. Figure 5a shows the elongated and irregular shape of the TiO<sub>2</sub> particles, while Figure 5b shows that the CuO particles has a rounded and more homogeneous shape.

**Figure 5.** SEM images of the (a) TiO<sub>2</sub> and (b) CuO particles.

The FTIR results obtained for MK, GP, and GP-G are shown in Figure 6. In the MK spectrum, a large band corresponding to asymmetric vibrations, specifically, vibrations of the Si–O–Si and O–Si–O groups, was centered at  $1089\text{ cm}^{-1}$  [43]. The band located at  $814\text{ cm}^{-1}$  was associated with the vibrational mode of the Al–O bond of the Al<sup>IV</sup> present in MK [43,44].

When MK was activated under alkaline conditions to form a geopolymer, the main bands at wavenumbers of  $1007$  and  $1015\text{ cm}^{-1}$  shifted in both the GP and GP-G mortar spectra; this band corresponded to the asymmetric vibration of the Si–OT bonds in the GP gel potassium aluminum silicate hydrates (KASH) (where T corresponds to Si or Al tetrahedrons) [45]. According to Tchakouté et al. [46], the infrared absorption bands at wavenumbers close to  $1100\text{ cm}^{-1}$  and  $950\text{ cm}^{-1}$  could indicate that the geopolymers contained more SiQ<sup>3</sup> and SiQ<sup>2</sup> species, respectively. Additionally, the band observed in the GP-G mortar spectrum was more intense than that observed in the GP spectrum, indicating the presence of more undissolved silica in the alkaline system [43]. This result was expected, since the mortar was designed with particles of G. The band located at approximately  $703\text{ cm}^{-1}$  came from symmetric vibrations of the presence of Ti–O–Ti photoactive species [10].

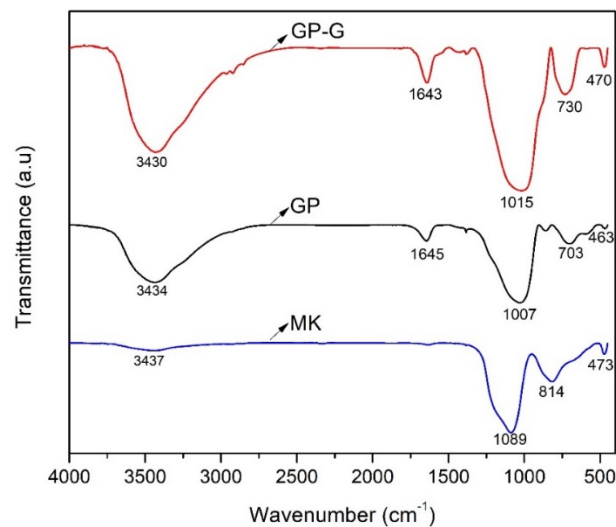


**Figure 6.** Fourier-transform infrared (FTIR) spectra obtained for MK, GP, and GP-G.

The peaks at approximately  $3434\text{ cm}^{-1}$  and  $1645\text{ cm}^{-1}$  in the MK, GP, and GP-G spectra corresponded to stress vibrations of the H–OH group, indicating that water molecules were associated with free water [38,47–49]. Finally, the peaks corresponding to the bending vibration of the Si–O–Si group [47,49] were identifiable at  $473$ ,  $463$ , and  $470\text{ cm}^{-1}$  for the MK, GP, and GP-G samples, respectively.

The SEM images of GP and GP-G are shown in Figure 7. Figure 7a shows that the GP had a smooth and homogeneous surface, indicating the presence of large amounts of the KASH gel. Unreacted MK that was not dissolved by the alkaline activation conditions was also identified [11,44,47]. GP showed a homogeneous distribution of the  $\text{TiO}_2$  nanoparticles inside the matrix. In a previous study [11], the effect of the incorporation of  $\text{TiO}_2$  in the geopolymeric matrix was investigated, and it was noteworthy that there was no significant difference between the morphologies of the systems with and without  $\text{TiO}_2$ , and that the formation of the KASH gel was not impeded by the addition of  $\text{TiO}_2$ , as these coexisted in the structure of the material. Comparing the physical properties (Table 3) of the geopolymer matrix [11], with and without  $\text{TiO}_2$  addition, we found that the water absorption decreased by just 3.9%, and the density and volume of the permeable pores increased by 5.73% and 1.52%, respectively.

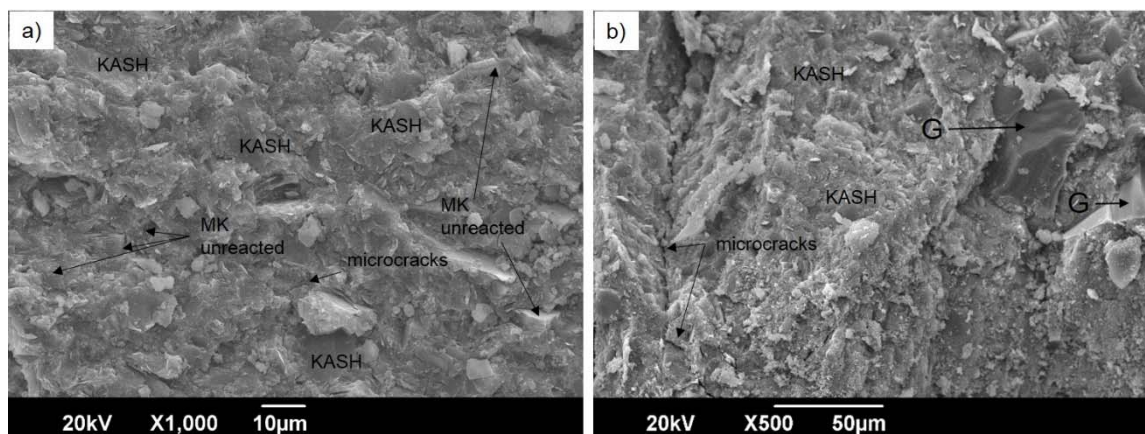


**Figure 7.** SEM images of the samples with 10 wt.%  $\text{TiO}_2$ : (a) GP and (b) GP-G mortar.

The glass particles of the GP-G mortar (Figure 7b) were identifiable by their large sizes and angular smooth surfaces [41,47], which were due to the milling processes that these particles underwent. The presence of micro-cracks in the sample was also observed with the incorporation of glass (Figure 7b); similar results were reported by Lin et al. [47] and Mejía de Gutiérrez et al. [41]. The GP-G had a more homogeneous and denser surface similar to that reported by Lin et al. [47] and a higher density (see Table 3); the material was more compact, which was reflected in its lower water absorption capacity and lower volume of permeable pores.

**Table 3.** Physical properties of the GP and GP-G samples.

Sample	Paste without TiO <sub>2</sub> [11]	GP (Paste) (10 wt.% TiO <sub>2</sub> )	GP-G (Mortar) (10 wt.%TiO <sub>2</sub> + G)
Absorption after immersion (%)	27.25 ± 0.15	26.18 ± 0.42	11.54 ± 0.26
Dry density (kg/m <sup>3</sup> )	1291 ± 0.25	1365 ± 0.02	1916 ± 140
Volume of permeable pores (%)	36.18 ± 0.34	36.73 ± 0.90	22.78 ± 1.97

### 3.2. Assays with Bacteria

Figure 8 shows the results of the first experimentation stage, corresponding to the standardization method using Petri dishes and exposure in nutrient agar with the GP and mGP. As shown in Figure 8a, for the mGP, no inhibition halo was observed for *E. coli*. Although authors such as Román et al. [15] showed the capacity of CuO nanoparticles to eliminate *Ochrobactrum anthropi*, in the present study and under the composition used (5 wt.% CuO), CuO geopolymeric compounds with antibacterial capacity for *E. coli*, *S. aureus*, and *P. aeruginosa* were not obtained.

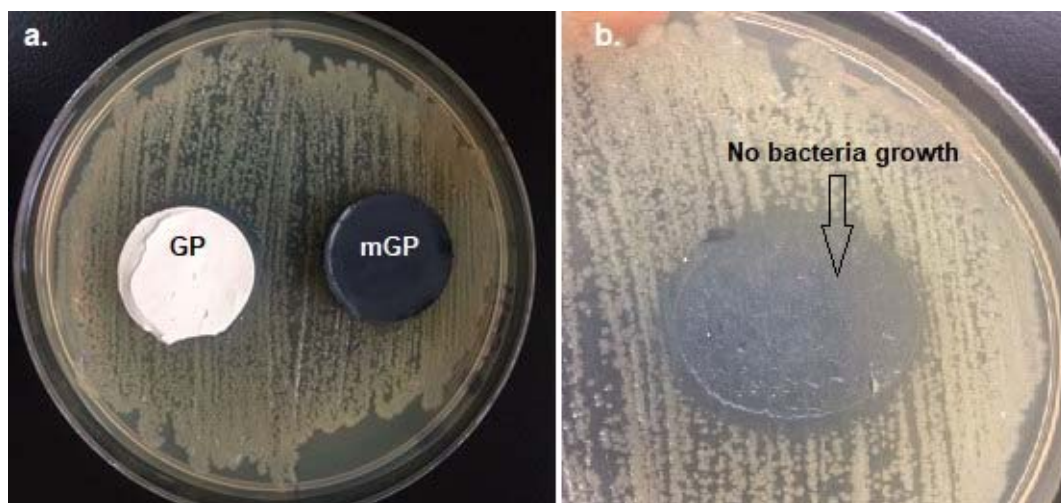


**Figure 8.** Standardization test for *Escherichia coli*: (a) GP (10 wt.% TiO<sub>2</sub>) and mGP (5 wt.% CuO); (b) inhibition of growth of bacteria under GP sample.

Previous studies demonstrated that the quantity of nanoparticles is an important parameter. The entrapment and inhibition of bacteria on surfaces was evaluated using CuO and Ag nanoparticles [2,22,33,34,42], and a good compatibility was reported in orthodontic adhesives using CuO in high quantities [17]. The amount of CuO nanoparticles used in this preliminary study was probably low and, for this reason, it did not allow for bacterial elimination. This is according to Guo et al. [14], who evaluated different percentages of TiO<sub>2</sub> in coatings fabricated by immersion and reported that an incorporation of 5 wt.% TiO<sub>2</sub> particles failed to eliminate *E. coli*, which was attributed to the processes of initial photocatalytic inactivation step being slow with this proportion of titanium oxide.

These nanoparticles were incorporated into materials because of their high surface/volume ratio, which allowed interactions with bacterial cell membranes, preventing these microorganisms from attaching to the material surface (bacteriostatic effect); when this occurred, the material was able to eliminate these microorganisms (bactericidal effect) [13,22–24,34]. Table 4 shows the results of the initial standardization assay for GP and mGP with the three bacteria tested.

**Table 4.** Results of the first bactericidal test phase: standardization method.

Sample	Bacteria/Formation of Halo/Halo Size		
	<i>Staphylococcus aureus</i>	<i>Escherichia coli</i>	<i>Pseudomonas aeruginosa</i>
GP	No—0	Yes—0.5 mm	No—0
mGP	No—0	No—0	No—0

In the case of the geopolymer with TiO<sub>2</sub> nanoparticles (GP), the standardization results were satisfactory for *E. coli*, in which a bactericidal effect was in fact observed for the sample GP. The inhibition was satisfactory, and a halo did form around the sample (Figure 8a); additionally, when sample GP was removed from the agar nutrient, no bacteria were found under the sample, as shown in Figure 8b. On the contrary, for the mGP, the halo formation was not evidenced; when the mGP sample was removed from the agar nutrient, an appreciable number of colonies grew below it for the three bacteria tested.

Based on the preliminary results of the first phase of standardization, the study was continued exclusively with GP samples; additionally, a GP-G mortar was fabricated and tested. The decision to use a geopolymer mortar with glass to measure the bactericide capacity of the geopolymers was based on the results reported by Mejía de Gutiérrez et al. [41], who observed a higher photocatalytic efficiency for B-rhodamine degradation in compounds functionalized with TiO<sub>2</sub> when glass waste was used to prepare the geopolymer mortars. Likewise, studies by Sikora et al. [35] showed that the use of glass enhanced the photocatalytic activity for *E. coli* colony degradation, and elimination occurred in 30 min.

In the second phase, the number of CFUs was analyzed in different solutions for short times (4–5 h) and after one day in the agar with the *E. coli*, *P. aeruginosa*, and *S. aureus* bacteria.

Analyzing the GP-G mortar exposed to the different solutions for short times (Table 5) showed that, after 5 h, CFUs were not present in the 10<sup>-7</sup> mL solutions for the three bacteria evaluated. Evaluating *S. aureus* exposed to GP (Figure 9) for 4 h in all solutions showed CFU growth, while, for the GP-G in the 10<sup>-7</sup> solutions, zero CFUs were evident. However, the GP exhibited significant antimicrobial activity for only the 10<sup>-7</sup> solutions containing *P. aeruginosa* (Figure 9). The results reported in this study corresponding to GP and GP-G are satisfactory. The toxicity of nanoparticles for inhibiting bacterial growth was previously demonstrated for *S. aureus* using ZnO nanoparticles by Sikora [35], and for *E. coli* using CuO by Kumar [20] and TiO<sub>2</sub> by Sunada et al. [50]. Sunada et al. [50] explained that the photokilling reaction of *E. coli* cells using TiO<sub>2</sub> is initiated by a partial decomposition of the outer membrane, followed by an attack of the cytoplasmic membrane, resulting in cell death. In general, the adhesion of nanoparticles onto the cell wall and the membrane of the microorganisms produces morphological changes characterized by shrinkage of the cytoplasm and membrane detachment, finally leading to rupture of cell wall [51]. Additionally, the photocatalysis generates reactive oxygen species (ROS) and free radical species, contributing to an increase in the antibacterial potential of the nanoparticles [34,51,52].

For the agar solutions exposed to GP for longer times (Table 6), the greatest inhibition occurred in the 10<sup>-6</sup> solutions for *Pseudomonas aeruginosa* (Figure 10) and *E. coli* (Figure 11). The highest efficacy for the inhibition of CFU bacterial growth was evidenced by the GP-G mortar in the 10<sup>-6</sup> solutions for the three bacteria evaluated. This result confirms that the incorporation of glass wastes in geopolymeric compounds increased the photocatalytic capacity and the bactericidal effect of the MK-based geopolymer supplemented with TiO<sub>2</sub> and, therefore, improved the bacterial growth inhibition capacity on surfaces.

Finally, according to Tables 5 and 6, samples GP and GP-G showed a bacteriostatic effect depending on the bacteria and time.

Although TiO<sub>2</sub> and other nanoparticles previously attracted a lot of interest due to their antibacterial properties in different applications, according to the results, in general, samples containing glass wastes showed a higher bacteriostatic effect. The use of ground glass particles maximized the capacity for inhibiting CFU growth after 5 h for the GP-G mortars in solutions of 10<sup>-7</sup> mL containing the three bacteria evaluated (*S. aureus*, *P. aeruginosa*, and *E. coli*). Furthermore, GP-G seems to be particularly effective against *P. aeruginosa*.

**Table 5.** Bacterial growth inhibition capacity of GP geopolymers (4 h) and GP-G (5 h) in bacteria-rich agar solutions.

Sample, Time in Agar	Dissolutions (mL)	CFU *		
		<i>S. aureus</i>	<i>P. aeruginosa</i>	<i>E. coli</i>
GP, 4 h	10 <sup>-3</sup>	++	++	++
	10 <sup>-4</sup>	++	++	++
	10 <sup>-5</sup>	++	+	+
	10 <sup>-6</sup>	+	+	+
	10 <sup>-7</sup>	+	–	+
	10 <sup>-8</sup>	+	–	+
GP-G, 5 h	10 <sup>-3</sup>	+	+	+
	10 <sup>-4</sup>	+	+	+
	10 <sup>-5</sup>	+	+	+
	10 <sup>-6</sup>	+	+	–
	10 <sup>-7</sup>	–	–	–
	10 <sup>-8</sup>	–	–	–

\* (+), bacterial growth determined by CFUs; (++) , bacterial growth determined by the formation of large colonies in all areas; (–), inhibition of bacterial growth.

**Table 6.** Bacterial growth inhibition capacity of GP (24 h) and GP-G (25 h) in bacteria-rich agar solutions.

Sample, Time in Agar	Dissolutions (mL)	Bacteria		
		<i>S. aureus</i>	<i>P. aeruginosa</i>	<i>E. coli</i>
GP, 24 h	10 <sup>-3</sup>	++	++	++
	10 <sup>-4</sup>	++	++	+
	10 <sup>-5</sup>	++	+	+
	10 <sup>-6</sup>	+	–	–
	10 <sup>-7</sup>	+	–	–
	10 <sup>-8</sup>	–	–	–
GP-G, 25 h	10 <sup>-3</sup>	+	+	+
	10 <sup>-4</sup>	+	–	+
	10 <sup>-5</sup>	+	–	+
	10 <sup>-6</sup>	–	–	–
	10 <sup>-7</sup>	–	–	–
	10 <sup>-8</sup>	–	–	–

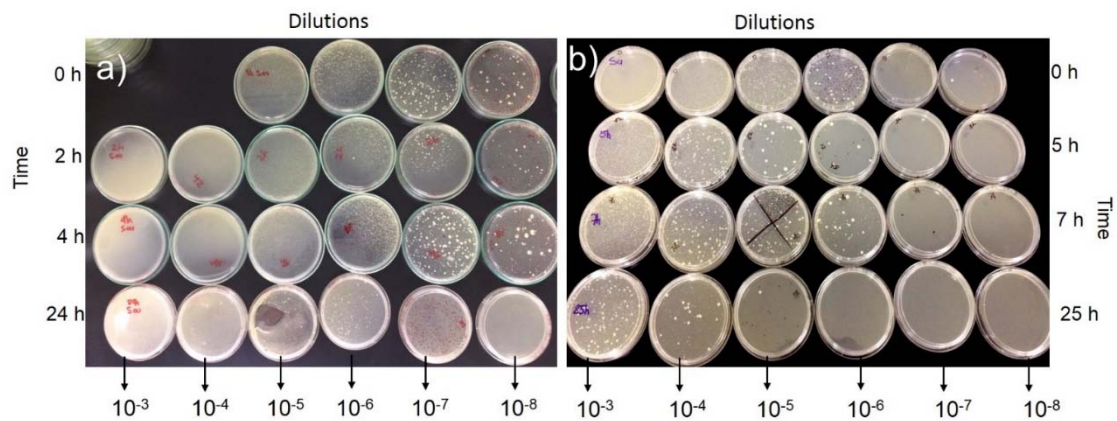


**Figure 9.** Reduction in the number of viable bacteria over time in the *S. aureus* agar for (a) GP and (b) GP-G.

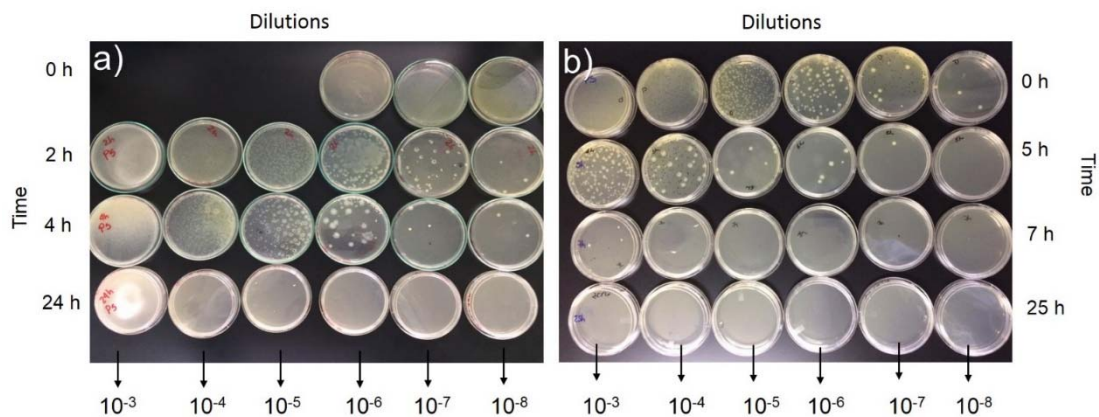


**Figure 10.** Reduction in the number of viable bacteria over time in the *P. aeruginosa* agar for (a) GP and (b) GP-G.

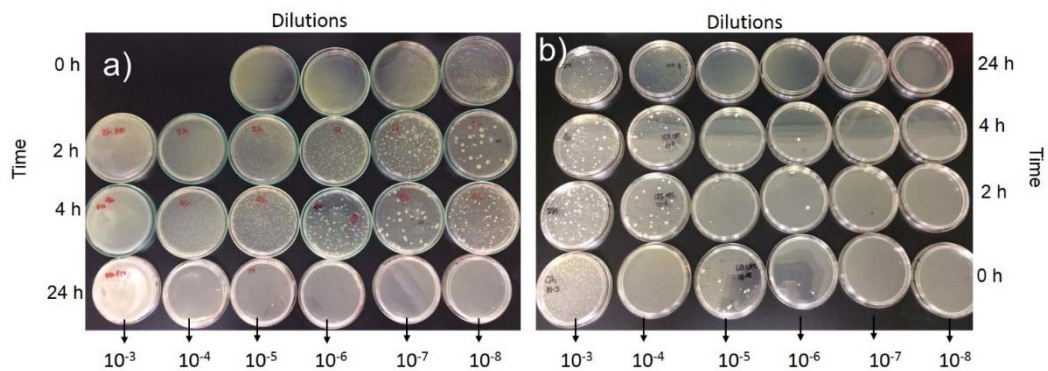


**Figure 11.** Reduction in the number of viable bacteria over time in the *E. coli* agar for (a) GP and (b) GP-G.

#### 4. Conclusions

Geopolymer composites based on the alkaline activation of MK and nanoparticles of  $\text{TiO}_2$  (10 wt.%) and  $\text{CuO}$  (5 wt.%) were produced. This study evaluated the physical and microstructural properties of the geopolymers and the functionality of these geopolymers for inhibiting the growth of the bacteria *S. aureus*, *P. aeruginosa*, and *E. coli*. Based on the results obtained, the following conclusions can be drawn:

- Here, 10 wt.% TiO<sub>2</sub> used for the manufacture of geopolymeric pastes and mortars showed satisfactory elimination of bacterial growth. In contrast, 5 wt.% CuO did not inhibit bacterial growth.
- The incorporation of glass wastes as fine aggregate endowed the GP-G with a 56.73% lower water absorption compared to the GP sample. Likewise, the glass particles endowed the material with a smoother and more homogeneous surface, 40.36% higher density, and 37.97% lower pore volume.
- The use of ground glass particles maximized the capacity for inhibiting CFU growth after 5 h for the GP-G mortars in solutions of 10<sup>-7</sup> mL containing the three bacteria evaluated (*S. aureus*, *P. aeruginosa*, and *E. coli*).
- After 24 h in the bacterial culture, the GP-G mortars exhibited a high capacity for inhibiting the growth of *P. aeruginosa* in the 10<sup>-4</sup> mL solutions and *E. coli* and *S. aureus* in the 10<sup>-6</sup> mL solutions.
- These results indicate the potential for using the MK-based geopolymer composite with 10 wt.% TiO<sub>2</sub> for applications on surfaces with antibacterial properties.

**Author Contributions:** Conceptualization, R.M.-d.G.; methodology, R.M.-d.G., M.V.-C. and M.A.; formal analysis, S.R.-B., M.A. and D.M.; investigation, R.M.-d.G., M.V.-C. and M.A.; resources, project administration and funding acquisition, R.M.-d.G.; writing—original draft preparation, M.V.-C. and S.R.-B.; writing—review and editing, R.M.-d.G. and M.V.-C. All authors have read and agreed to the published version of the manuscript.

**Funding:** This research was funded by Universidad del Valle (Cali, Colombia), grant number 139-2017.

**Conflicts of Interest:** The authors declare no conflict of interest.

## References

1. Ang, T.; He, Y.; Xiangxin, X.; Yong, L. Antibacterial Ceramic Fabricated by the Ti-Bearing Blast Furnace Slag. In Proceedings of the 8th Pacific Rim International Congress on Advanced Materials and Processing, Hilton Waikoloa Village in Waikoloa, HI, USA, 4–9 August 2013; Marquis, F., Ed.; Springer: Cham, Switzerland, 2016; pp. 1627–1634.
2. Baheiraei, N.; Moztarzadeh, F.; Hedayati, M. Preparation and antibacterial activity of Ag/SiO<sub>2</sub> thin film on glazed ceramic tiles by sol-gel method. *Ceram. Int.* **2012**, *38*, 2921–2925. [[CrossRef](#)]
3. Wang, L.; Hu, C.; Shao, L. The antimicrobial activity of nanoparticles: Present situation and prospects for the future. *Int. J. Nanomed.* **2017**, *12*, 1227–1249. [[CrossRef](#)] [[PubMed](#)]
4. Salgado, C.D.; Farr, B.M.; Calfee, D.P. Community-Acquired Methicillin-Resistant Staphylococcus aureus: A Meta-Analysis of Prevalence and Risk Factors. *Clin. Infect. Dis.* **2003**, *36*, 131–139. [[CrossRef](#)]
5. Gelatti, L.C.; Bonamigo, R.R.; Matsiko-Inoue, F.M.; Do-Carmo, S.; Becker, A.P.; Da Silva-Castrucci, F.M.; Campos Pignatari, A.C.; Dazevedo, P.A. Community-acquired methicillin-resistant staphylococcus aureus carrying scmec type IV in southern Brazil. *Rev. Soc. Bras. Med. Trop.* **2013**, *46*, 34–38. [[CrossRef](#)]
6. Drugă, B.; Ukrainczyk, N.; Weise, K.; Koenders, E.; Lackner, S. Interaction between wastewater microorganisms and geopolymer or cementitious materials: Biofilm characterization and deterioration characteristics of mortars. *Int. Biodeterior. Biodegrad.* **2018**, *134*, 58–67. [[CrossRef](#)]
7. Crocker, J. Antibacterial Materials. *Mater. Sci. Technol.* **2007**, *22*, 238–241. [[CrossRef](#)]
8. Abdel-Gawwad, H.A.; Mohamed, S.A.; Mohammed, M.S. Recycling of slag and lead-bearing sludge in the cleaner production of alkali activated cement with high performance and microbial resistivity. *J. Clean. Prod.* **2019**, *220*, 568–580. [[CrossRef](#)]
9. Hasmaliza, M.; Foo, H.S.; Mohd, K. Anatase as Antibacterial Material in Ceramic Tiles. *Procedia Chem.* **2016**, *19*, 828–834. [[CrossRef](#)]
10. Dahiya, M.S.; Tomer, V.K.; Duhan, S. Bioactive glass/glass ceramics for dental applications. In *Applications of Nanocomposite Materials in Dentistry*; Abdullah, M., Mohammad, I., Mohammad, A., Eds.; Woodhead Publishing Series in Biomaterials: Cambridge, UK, 2018; pp. 1–25.
11. Guzmán-Aponte, L.; Mejía de Gutiérrez, R.; Maury-Ramírez, A. Metakaolin-Based Geopolymer with Added TiO<sub>2</sub> particles: Physicomechanical Characteristics. *Coatings* **2017**, *7*, 233. [[CrossRef](#)]
12. Mohd Adnan, M.A.; Muhd Julkapli, N.; Amir, M.N.I.; Maamor, A. Effect on different TiO<sub>2</sub> photocatalyst supports on photodecolorization of synthetic dyes: A review. *Int. J. Environ. Sci. Technol.* **2019**, *16*, 547–566. [[CrossRef](#)]

13. Rai, M.; Yadav, A.; Gade, A. Silver nanoparticles as a new generation of antimicrobial. *Biotechnol. Adv.* **2009**, *27*, 76–83. [[CrossRef](#)] [[PubMed](#)]
14. Ming-Zhi, G.; Tung-Chai, L.; Chi-Sun, P. Nano-TiO<sub>2</sub>-based architectural mortar for NO removal and bacteria inactivation: Influence of coating and weathering conditions. *Cem. Concr. Compos.* **2013**, *36*, 101–108.
15. Román, L.E.; Castro, F.; Maúrtua, D.; Condori, C.; Vivas, D.; Bianclii, A.E.; Paraguay-Delgado, F.; Solis, J.L.; Gómez, M.M. CuO nanoparticles and their antimicrobial activity against nosocomial strains. *Rev. Colomb. Quim.* **2017**, *46*, 28–36.
16. Sikora, P.; Augustyniak, A.; Cendrowski, K.; Nawrotek, P.; Mijowska, E. Antimicrobial activity of Al<sub>2</sub>O<sub>3</sub>, CuO, Fe<sub>3</sub>O<sub>4</sub>, and ZnO nanoparticles in scope of their further application in cement-based building materials. *Nanomaterials* **2018**, *8*, 212. [[CrossRef](#)] [[PubMed](#)]
17. Toodehzaeim, M.H.; Zandi, H.; Meshkani, H.; Hosseinzadeh Firouzabadi, A. The Effect of CuO Nanoparticles on Antimicrobial Effects and Shear Bond Strength of Orthodontic Adhesives. *J. Dent.* **2018**, *19*, 1–5.
18. Yang, S.; Zhang, Y.; Yu, J.; Zhen, Z.; Huang, T.; Tang, Q.; Chu, P.K.; Qi, L.; Lv, H. Antibacterial and mechanical properties of honeycomb ceramic materials incorporated with silver and zinc. *Mater. Des.* **2014**, *59*, 461–465. [[CrossRef](#)]
19. Haider, A.J.; Anbari, R.; Kadhim, G.R.; Salame, C.T. Exploring potential environmental applications of TiO<sub>2</sub> nanoparticles. *Energy Procedia* **2017**, *119*, 332–345. [[CrossRef](#)]
20. Kumar, A.M.; Khan, A.; Suleiman, R.; Qamar, M.; Saravanan, S.; Dafalla, H. Bifunctional CuO/TiO<sub>2</sub> nanocomposite as nanofiller for improved corrosion resistance and antibacterial protection. *Prog. Org. Coat.* **2018**, *114*, 9–18. [[CrossRef](#)]
21. Mersian, H.; Alizadeh, M.; Hadi, N. Synthesis of zirconium doped copper oxide (CuO) nanoparticles by the Pechini route and investigation of their structural and antibacterial properties. *Ceram. Int.* **2018**, *44*, 20399–20408. [[CrossRef](#)]
22. Armayani, M.; Pratama, M.A. The Properties of Nano Silver (Ag)-Geopolymer as Antibacterial Composite for Functional Surface Materials. *Matec. Web Conf.* **2017**, *97*, 01010. [[CrossRef](#)]
23. Elbourne, A.; Crawford, R.J.; Ivanova, E.P. Nano-structured antimicrobial surfaces: From nature to synthetic analogues. *J. Colloid Interface Sci.* **2017**, *508*, 603–616. [[CrossRef](#)] [[PubMed](#)]
24. Dizaj, S.M.; Lotfipour, F.; Barzegar-Jalali, M.; Zarrintan, M.H.; Adibkia, K. Antimicrobial activity of the metals and metal oxide nanoparticles. *Mater. Sci. Eng. C* **2014**, *44*, 278–284. [[CrossRef](#)] [[PubMed](#)]
25. Åsbrink, S.; Norrby, L.J. A refinement of the crystal structure of copper (II) oxide with a discussion of some exceptional. *Acta. Crystallogr. Sect. B* **1970**, *26*, 8–15. [[CrossRef](#)]
26. Mejía, J.M.; Mendoza, J.D.; Yucuma, J.; Mejía de Gutiérrez, R.; Mejía, D.E.; Astudillo, M. Mechanical, in-vitro biological and antimicrobial characterization as an evaluation protocol of a ceramic material based on alkaline activated metakaolin. *Appl. Clay Sci.* **2019**, *178*, 105141. [[CrossRef](#)]
27. Falah, M.; MacKenzie, K.J.D. Synthesis and properties of novel photoactive composites of P25 titanium dioxide and copper (I) oxide with inorganic polymers. *Ceram. Int.* **2015**, *41*, 13702–13708. [[CrossRef](#)]
28. Syamsidar, D.; Nurfadilla, S. The Properties of Nano TiO<sub>2</sub>-Geopolymer Composite as a Material for Functional Surface Application. *MATEC Web Conf.* **2017**, *97*, 01013. [[CrossRef](#)]
29. Rodrigues Magalhaes, A.P.; Laura, B.S.; Gonzaga Lopes, L.; Rodrigues de Araujo, E.; Estrela, C.; Torres, E.M.; Figueiroa Bakuzis, A.; Carvalho Cardoso, P.; Santos Carriao, M. Nanosilver Application in Dental Cements. *ISRN Nanotechnol.* **2012**, *2012*, 6. [[CrossRef](#)]
30. Wu, Y.; Lu, B.; Bai, T.; Wang, H.; Du, F.; Zhang, Y.; Cai, L.; Jiang, C.; Wang, W. Review. Geopolymer, green alkali activated cementitious material: Synthesis, applications and challenges. *Constr. Build. Mater.* **2019**, *224*, 930–949. [[CrossRef](#)]
31. Mondragón-Figueroa, M.; Guzmán-Carrillo, H.; Rico, M.A.; Reytez-Araiza, J.L.; Pineda-Piñón, J.; López-Naranjo, E.J.; Columba-Palomares, M.C.; López-Romero, J.M.; Gasca-Tirado, J.R.; Manzano-Ramírez, A. Development of a Construction Material for Indoor and Outdoor, Metakaolinite-Based Geopolymer, with Environmental Properties. *J. Mater. Sci. Eng. A* **2019**, *9*, 131–142.

32. Nur, Q.A.; Sari, N.U.; Harianti, S. Development of Geopolymers Composite Based on Metakaolin-Nano ZnO for Antibacterial Application. *IOP Conf. Ser. Mater. Sci. Eng.* **2017**, *180*, 012289. [[CrossRef](#)]
33. Dela Cerna, K.; Janairo, J.I.; Promentilla, M.A. Development of nanosilver-coated geopolymer beads (AgGP) from fly ash and baluko shells for antimicrobial applications. *MATEC Web Conf.* **2019**, *268*, 05003. [[CrossRef](#)]
34. Dibyendu, A.; Manas, S.; Moumita, M.; Abiral, T.; Saroj, M.; Brajadulal, C.H. Anti-microbial efficiency of nano silver–silica modified geopolymer mortar for eco-friendly green construction technology. *RSC Adv.* **2015**, *5*, 64037.
35. Sikora, P.; Augustyniak, A.; Cendrowski, K.; Horszczaruk, E.; Rucinska, T.; Nawrotek, P.; Mijowska, E. Characterization of mechanical and bactericidal properties of cement mortars containing waste glass aggregate and nanomaterials. *Materials (Basel)* **2016**, *9*, 701. [[CrossRef](#)] [[PubMed](#)]
36. Centers for Disease Control & Prevention. Four Pediatric Deaths from Community-Acquired Methicillin-Resistant Staphylococcus aureus—Minnesota and North Dakota 1997–1999. *Morb. Mortal. Wkly. Rep.* **1999**, *48*, 707–710.
37. Van Elsas, J.D.; Semenov, A.V.; Costa, R.; Trevors, J.T. Survival of Escherichia coli in the environment: Fundamental and public health aspects. *ISME J.* **2011**, *5*, 173–183. [[CrossRef](#)]
38. Villaquirán-Caicedo, M.A. Studying different silica sources for preparation of alternative waterglass used in preparation of binary geopolymer binders from metakaolin/boiler slag. *Constr. Build. Mater.* **2019**, *227*, 116621. [[CrossRef](#)]
39. Villaquirán-Caicedo, M.A.; Mejía-de Gutiérrez, R. Mechanical and microstructural analysis of geopolymer composites based on metakaolin and recycled silica. *J. Am. Ceram. Soc.* **2019**, *102*, 3653–3662. [[CrossRef](#)]
40. Sunde, T.O.L.; Grande, T.; Einarsrud, M.A. Modified Pechini Synthesis of Oxide Powders and Thin Films. In *Handbook of Sol-Gel: Science and Technology*; Klein, L., Aparicio, M., Jitianu, A., Eds.; Springer: Cham, Switzerland, 2016; pp. 1–30.
41. Mejía de Gutiérrez, R.; Villaquirán-Caicedo, M.A.; Guzmán-Aponte, L. Alkali-activated metakaolin mortars using glass waste as fine aggregate: Mechanical and photocatalytic properties. *Constr. Build. Mater.* **2020**, *235*, 117510. [[CrossRef](#)]
42. Akl, A.; Nida, M. Antibacterial Activity of synthesized Copper Oxide Nanoparticles using Malva sylvestris Leaf Extract. *SMU Med. J.* **2015**, *2*, 91–101.
43. Bernal, S.A.; Rodríguez, E.D.; Mejía de Gutierrez, R.; Provis, J.L.; Delvasto, S. Activation of Metakaolin/Slag Blends Using Alkaline Solutions Based on Chemically Modified Silica Fume and Rice Husk Ash. *Waste Biomass Valoriz.* **2011**, *3*, 99–108. [[CrossRef](#)]
44. Villaquiran-Caicedo, M.A.; Mejía de Gutiérrez, R. Synthesis of ternary geopolymers based on metakaolin, boiler slag and rice husk ash. *Dyna* **2015**, *82*, 104–110. [[CrossRef](#)]
45. Arellano-Aguilar, R.; Burciaga-Díaz, O.; Gorokhovskiy, A.; Escalante-García, J.I. Geopolymer mortars based on a low grade metakaolin: Effects of the chemical composition, temperature and aggregate:binder ratio. *Constr. Build. Mater.* **2014**, *50*, 642–648. [[CrossRef](#)]
46. Tchakouté, H.K.; Rüschler, C.H.; Kong, S.; Kamseu, E.; Leonelli, C. Geopolymer binders from metakaolin using sodium waterglass from waste glass and rice husk ash as alternative activators: A comparative study. *Constr. Build. Mater.* **2016**, *114*, 276–289. [[CrossRef](#)]
47. Lin, K.L.; Shiu, H.S.; Shie, J.L.; Cheng, T.W.; Hwang, C.L. Effect of composition on characteristics of thin film transistor liquid crystal display (TFT-LCD) waste glass-metakaolin-based geopolymers. *Constr. Build. Mater.* **2012**, *36*, 501–507. [[CrossRef](#)]
48. Elimbi, A.; Tchakouté, H.K.; Njopwouo, D. Effects of calcination temperature of kaolinite clays on the properties of geopolymer cements. *Build. Mater.* **2011**, *25*, 2805–2812. [[CrossRef](#)]
49. Covarrubias, C.; García, R.; Arriagada, R.; Yáñez, J.; Garland, M.T. Cr (III) exchange on zeolites obtained from kaolin and natural mordenite. *Microporous Mesoporous Mater.* **2006**, *88*, 220–231. [[CrossRef](#)]
50. Sunada, K.; Watanabe, T.; Hashimoto, K. Studies on photokilling of bacteria on TiO<sub>2</sub> thin film. *J. Photochem. Photobiol. A: Chem.* **2003**, *156*, 227–233. [[CrossRef](#)]

51. Dakal, T.C.; Kumar, A.; Majumdar, R.S.; Yadav, V. Mechanistic basis of antimicrobial actions of silver nanoparticles. *Front. Microbiol.* **2016**, *7*, 1–17. [[CrossRef](#)]
52. Marugan, J.; Grieken, R.V.; Pablos, C.; Sordo, C. Analogies and differences between photocatalytic oxidation of chemicals and photocatalytic inactivation of microorganisms. *Water Res.* **2010**, *44*, 789–796. [[CrossRef](#)]



© 2020 by the authors. Licensee MDPI, Basel, Switzerland. This article is an open access article distributed under the terms and conditions of the Creative Commons Attribution (CC BY) license (<http://creativecommons.org/licenses/by/4.0/>).